X-Ray Image Enhancement Using Blind Denoising Neural Networks

Wei Yin
Hwamei Hospital, University of Chinese Academy of Sciences, Ningbo 315010, China
Ningbo Institute of Life and Health Industry, University of Chinese Academy of Sciences, Ningbo 315010, China
yinwei@ucas.ac.cn

Baolian Qi
Hwamei Hospital, University of Chinese Academy of Sciences, Ningbo 315010, China
Ningbo Institute of Life and Health Industry, University of Chinese Academy of Sciences, Ningbo 315010, China
qibaolian@ucas.ac.cn

Ting Cai
Hwamei Hospital, University of Chinese Academy of Sciences, Ningbo 315010, China
Ningbo Institute of Life and Health Industry, University of Chinese Academy of Sciences, Ningbo 315010, China
caiting@ucas.ac.cn

Jinpeng Li*, Member, IEEE
Hwamei Hospital, University of Chinese Academy of Sciences, Ningbo 315010, China
Ningbo Institute of Life and Health Industry, University of Chinese Academy of Sciences, Ningbo 315010, China
lijinpeng@ucas.ac.cn

2021 IEEE International Conference on Artificial Intelligence and Computer Applications (ICAICA) | 978-1-6654-1867-6/21/$31.00 ©2021 IEEE | DOI: 10.1109/ICAICA52286.2021.9497945

***Abstract*—X-ray imaging is a common medical imaging technology, which plays an important role in assisting doctors in diagnosis. However, the quality of X-ray images is often disturbed by noise in practical applications, which affects the diagnosis of the disease. Although several works have discussed the X-ray images denoising algorithms, their performance needs further improvement. In order to improve the quality of X-ray images, we propose a blind denoising algorithm based on convolutional neural network (X-BDCNN) with a more reasonable noise model. The noise model is designed according to the physical principle of the X-ray imaging, which can generate more realistic noisy X-ray images for training. X-BDCNN consists of a noise level estimation subnetwork and a non-blind denoising subnetwork. The noise level estimation subnetwork estimates the noise level of input noisy image so as to promote the performance of denoised image in the other subnetwork. Additionally, we add a SSIM loss function for X-BDCNN to further improve the quality of denoised images. The experiments under different noise levels demonstrate that our X-BDCNN has a superior performance in various evaluation metrics compared with existing denoising methods.**

Keywords—image enhancement, image denoising, hybrid noise, X-ray images, convolutional neural networks

I. Introduction

X-ray is widely used in disease diagnosis, such as pneumonia, bone fracture, congestive heart failure and tuberculosis. Although X-ray imaging plays an important role in medical diagnosis, the quality of X-ray images is influenced by various types and levels of noise during imaging phase, which may affect doctors' diagnosis and analysis of the disease. Thus, it is necessary to improve the quality of X-ray images. There are two main lines of methods to achieve this goal. One is increasing the radiation dosage or exposure time. However, recent researches have shown that some risks may be increased in high radiation dosage, such as the chance of developing cancer [1]. The other method is to use image denoising algorithms to restore the quality of X-ray images collected at low radiation dosage. For the sake of protecting both doctors and patients from side effect, low radiation dosage of X-rays are usually used. However, in low radiation dosage, reducing incident photon density and photon unevenness will lead to a much higher quantum noise (also called photon noise, shot noise or Poisson noise) which is a signal-dependent noise. Meanwhile, the common thermal noise produced by X-ray sensors and other electronic devices will further corrupt X-ray images, which is a signal-independent noise [2]. To promote the practical application of X-ray in low radiation dosage, it is necessary to reduce the noise and improve the quality of X-ray images.

In the early years, many image denoising methods for additive white Gaussian noise have been applied to deal with the noise of X-ray images, such as total variation regularized method [3], non-local means [4] and block matching and 3D filtering (BM3D) [5]. However, the same performance in noise reduction is difficult to obtain with these methods due to ignoring the noise component of X-ray images.

According to the characteristic of X-ray imaging systems, the signal related quantum noise has a bigger impact on images than the thermal noise. To overcome the influence of Poisson noise, a Poisson non-local principle component analysis method [6] has been proposed to improve the image quality of photon-limited imaging systems. The variance stabilizing transform (VST) [7] is an effective method for Poisson noise. The VST-based methods first transfer Poisson noise into a signal independent Gaussian noise, and then the denoising algorithms for Gaussian noise can be used to reduce the noise. The final restored image will be obtained by an inverse VST. However, since the VST-based methods ignore the Gaussian noise component of X-ray images, they can't achieve good performance.

Recent studies reveal that deep learning has a great potential on image denoising. For example, Zhang et al. [8] adopts a deep convolutional neural network (DnCNN) to remove Gaussian noise and obtain a state-of-the-art performance. Furthermore, Guo et al. [9] proposes a convolutional blind denoising network (CBDNet) for real-world noisy photographs based on a more realistic noise model. Recently, some denoising approaches of X-ray images based on deep learning have been proposed, such as X-ReCNN [10] and SkiDNet [11]. However, it is necessary to develop new methods because these methods ignore the

formation mechanism of noise in X-ray images.

To ensure the high-quality performance of noise reduction for X-ray images, this work proposes a blind denoising algorithm based on convolutional neural network for X-ray images (X-BDCNN). X-BDCNN is comprised with a noise level estimation (NLE) subnetwork and a non-blind denoising (NBD) subnetwork. The NLE subnetwork estimates the noise level from input X-ray images and the estimated noise level will be fed to the NBD subnetwork.

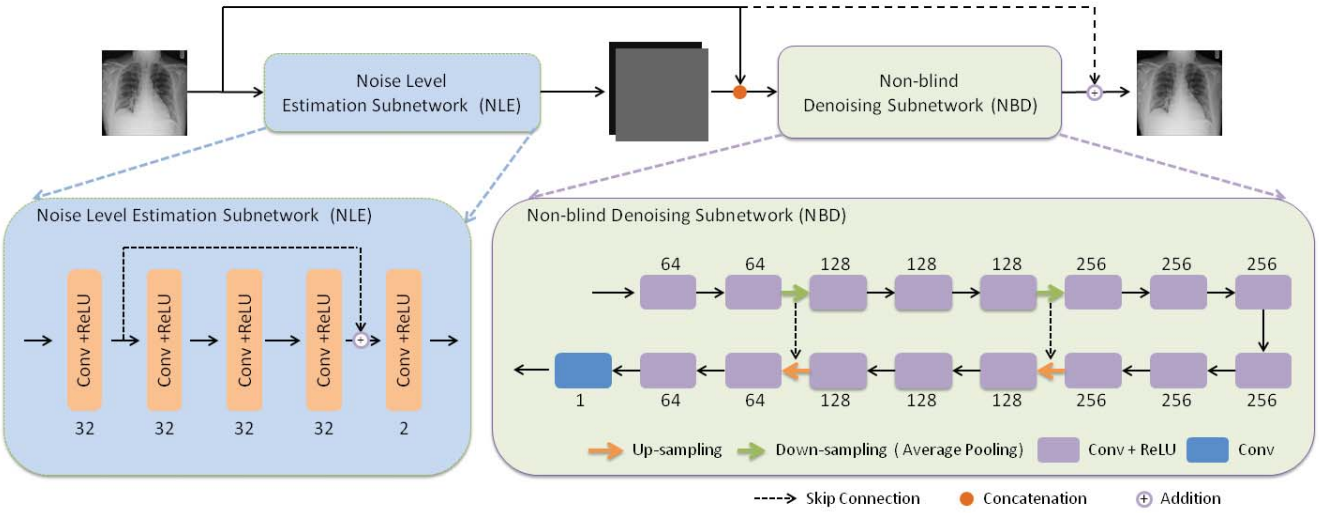

Fig. 1. The architecture of X-BDCNN. The NLE subnetwork estimates the noise level from the input noisy image, and the NBD subnetwork takes both the noisy image and the estimated noise level as input to predict the final noise-free image.

Since the distribution of synthetic noises will significantly influence the performance of denoising methods , we use a more reasonable noise model in line with X-ray imaging systems to synthesize the training data.

The main contribution of this paper is threefold:

1) A realistic hybrid Poisson-Gaussian noise model is proposed. More specifically, the model synthesizes realistic noisy images that can better characterize the real X-ray noise.
2) A noise level estimation subnetwork is designed to estimate the level of Poisson noise and Gaussian noise, which is helpful for improving the performance of denoising.
3) SSIM is integrated into the loss function to preserve the structural information of the images, which is important to X-ray diagnosis.

II. Proposed Method

A. Hybrid Poisson-Gaussian Noise Model

Most of denoising methods of X-ray images are trained for Gaussian noise or Poisson noise and they generally do not work well on real noisy image of X-ray. Thus, a more reasonable noise model for X-ray images needs to be built. As indicated in [2], the X-ray imaging systems generally suffer from two kind of noise, quantum noise and thermal noise. Thus, we use a hybrid Poisson-Gaussian noise model to simulate the degraded process of X-ray images, which is defined as

$$f(x,y) = p(x,y) + n(x,y), \tag{1}$$

where $f(x,y)$ represents the observed degraded X-ray images, $p(x,y)$ is the degraded image by Poisson noise, and $n(x,y)$ represents the thermal noise which is a signal-independent Gaussian noise with noise zero-mean and noise variance σ^2. The Poisson degraded process denotes that the intensity of $p(x,y)$ is drawn from a Poisson distribution with parameter $\lambda=g(x,y)$, where $g(x,y)$ is the latent noise-free image. The Poisson density distribution is defined as

$$P(p(x,y)=k) = \frac{\lambda^k e^{-\lambda}}{k!}. \tag{2}$$

Therefore, we can generate many noisy X-ray images in different noise levels to train our X-BDCNN depend on the hybrid Poisson-Gaussian noise model. As shown in Eq. (1), the σ can be used to control the intensity of Gaussian noise in X-ray images. The intensity of Poisson noise is related to the intensity of source images, we add a scale factor η to Eq. (2) and control the intensity of Poisson noise by η. Specifically, we use random. poisson function in Numpy to generate Poisson noisy image. In this work, σ and η are randomly sampled from the ranges of (0, 20) and (0.4, 1.9), respectively.

B. CNN-based Denoising Method

Network Architecture: According to the hybrid Poisson-Gaussian noise model, the intensity of Gaussian and Poisson noise in X-ray images is determined by the parameter σ and η respectively. Obviously, the known σ and η help promoting the quality of the denoised image from the observed noisy image. Motivated by this, we propose a novel neural network X-BDCNN (shown in Fig. 1). X-BDCNN consists of the NLE subnetwork and the NBD subnetwork. The NLE subnetwork can estimate the noise level maps $\hat{l}_{\sigma,\eta}(f) = \mathcal{F}_{NLE}(f;\mathrm{W}_{NLE})$ from the input observed image, where W_{NLE} is the parameters in the NLE subnetwork. Then,

the latent noise-free image $\hat{g} = \mathcal{F}_{NBD}\left(f, \hat{l}_{\sigma,\eta}(f); \mathrm{W}_{NBD}\right)$ can be obtained by fed both the noise level maps and the input image into the NBD subnetwork, where W_{NBD} represents the parameter in the NBD subnetwork. Furthermore, the NLE subnetwork comprises five convolution layers with a skip connection between the first and fourth layer, and each convolution layer is followed by a ReLu activation function. The feature channel and filter size are set to 32 and 3×3 in each layer, respectively. The NBD subnetwork adopts residual learning to learn the residual mapping $\mathcal{R}\left(f, \hat{l}_{\sigma,\eta}(f); \mathrm{W}_{NBD}\right)$ firstly and then the final noise-free image could be obtained by $\hat{g} = f + \mathcal{R}\left(f, \hat{l}_{\sigma,\eta}(f); \mathrm{W}_{NBD}\right)$. More specifically, the NBD subnetwork has 17 convolution layers and the first 16 layers are similar to a symmetric U-net [12] with two down-sampling layers and two up-sampling layers (shown in Fig. 1). The filter size is set to 3×3 in all convolution layers, and ReLU activation function is used after each convolution layer except the last convolution layer. In order to increase the receptive field and utilize the multi-scale information, skip connections and transpose convolutions (up-sampling layers) are used in the NBD subnetwork.

Loss Function: To improve the quality of the restored image, a mixed loss function is utilized to train X-BDCNN. As noted in [9], the non-blind denoising networks are often robust when the estimated noise level $\hat{l}_{\sigma,\eta}$ is more than the ground-truth noise level $\tilde{l}_{\sigma,\eta}$. Thus, we use a asymmetric mean square error (MSE) loss function $\mathcal{L}_{asymm}$ to constrain the estimation of $\hat{l}_{\sigma,\eta}$, which is defined as

$$\mathcal{L}_{asymm} = \sum |\alpha - \beta| (\hat{l}_{\sigma,\eta}(f) - \tilde{l}_{\sigma,\eta}(f))^2, \tag{3}$$

where $\beta = 1$ if $\hat{l}_{\sigma,\eta}(f) - \tilde{l}_{\sigma,\eta}(f)) < 0$ and 0 otherwise. To make the model generalize well to real noise, α is selected between 0 and 0.5 because it can impose more penalty to under-estimation error.

Based on the prior knowledge that the noise level map is very smooth, we add a total variation (TV) regularizer loss function $\mathcal{L}_{TV}$ to constrain the estimation of the noise level map.

$$\mathcal{L}_{TV} = \left\| \nabla_h \hat{l}_{\sigma,\eta}(f) \right\|_2^2 + \left\| \nabla_v \hat{l}_{\sigma,\eta}(f) \right\|_2^2, \tag{4}$$

where ∇_h, ∇_v is the gradient operator in the horizontal and vertical direction, respectively.

Meanwhile, we use a traditional MSE loss function for the output $\hat{g}$ of the NBD subnetwork, which is defined as

$$\mathcal{L}_{MSE} = \sum_{\mathrm{x} \in \Omega} (\hat{g}(\mathrm{x}) - g(\mathrm{x}))^2, \tag{5}$$

where $\hat{g}, g$ represents the estimated noise-free image and the ground-truth clean image, respectively.

To preserve the important structural information of restored X-ray images, we add the SSIM loss function $\mathcal{L}_{SSIM}$ [13] to train X-BDCNN.

$$\mathcal{L}_{SSIM} = \sum_{\mathrm{x} \in \Omega} 1 - \mathrm{SSIM}(\hat{g}(\mathrm{x}), g(\mathrm{x})). \tag{6}$$

The structural similarity (SSIM) is a common image evaluation method which can measure the similarity of two images. Its formula is defined as

$$\mathrm{SSIM}(\hat{g}, g) = \frac{\left(2\mu_{\hat{g}}\mu_g + C_1\right)\left(2\sigma_{\hat{g}g} + C_2\right)}{\left(\mu_{\hat{g}}^2 + \mu_g^2 + C_1\right)\left(\sigma_{\hat{g}}^2 + \sigma_g^2 + C_2\right)}, \tag{7}$$

where $\mu_{\hat{g}}$ and μ_g is the mean of image $\hat{g}$ and g, respectively. They represent the luminance information of the image. The $\sigma_{\hat{g}}^2$ and σ_g^2 is the variance of image $\hat{g}$ and g respectively, which represents the contrast information of the image. The $\sigma_{\hat{g}g}$ is the covariance between the image $\hat{g}$ and g, and it represents the similarity of structural information of the two images. Both C_1 and C_2 are positive constants.

Finally, the mixed loss functions of X-BDCNN can be written as

$$\mathcal{L} = \lambda_1 \mathcal{L}_{MSE} + \lambda_2 \mathcal{L}_{SSIM} + \lambda_3 \mathcal{L}_{asymm} + \lambda_4 \mathcal{L}_{TV}, \tag{8}$$

where $\lambda_i (i = 1, 2, 3, 4)$ is the trade-off parameter for different loss functions in Eq. (8), respectively.

III. Experiments and Results

To evaluate the performance of the proposed method, we choose four existing denoising methods to compare with X-BDCNN, *i.e.* BM3D [5], DnCNN [8], X-ReCNN [10]. The last method is proposed for X-ray images. To quantitatively evaluate the performance of X-BDCNN, we use three widely-used image quality evaluation methods to compare the quality of the restored images by different methods, *i.e.* Signal-to-noise ratio (SNR), Peak Signal Noise Ratio (PSNR) and SSIM.

A. Dataset and Training Details

The ChestX-ray8 [14] which includes 108,948 frontal-view chest X-ray images is used to evaluate our method. We randomly select 10,000 X-ray images in this dataset and randomly crop them into 128×128 patches (320,000 in total). Then, we use the proposed noise model to generate different synthetic noisy X-ray images and divide them into the Training Set, Validation Set and Test Set with the ratio 7:2:1. To train X-BDCNN, We first set the parameters $\alpha = 0.3$ in Eq. (3) and $\lambda_1 = 0.4, \lambda_2 = 0.6, \lambda_3 = 0.5, \lambda_4 = 0.05$ in Eq. (8). The Adam optimizer is used to minimize the loss functions of X-BDCNN. The learning rate is 10^{-3} in the first 20 epochs, and 10^{-4} in the last 20 epochs. It takes about 30

hours to train X-BDCNN with Pytorch package on a NVIDIA GeForce GTX 2080 Ti GPU and obtain a satisfactory denoising performance.

B. Results

Table I shows the quantitative metrics of the restored images by different methods on the Test Set. It can be found that X-BDCNN performs the best among the all denoising methods in the metrics of the average SNR, the average PSNR and the average SSIM. The second row is the average results between the noisy images and the original clean images. It is shown that the results of denoised images processed by these denoising methods have a significant improvement than before. And X-BDCNN has the best results among those denoising methods. As for the average running time, BM3D [5] is the slowest method, and X-ReCNN [10] is the fastest method. The average running time of X-BDCNN is only 0.002 second slow compared to the X-ReCNN [10]. This is partly due to that CNN-based method using GPU to accelerate and the network architecture of X-BDCNN is more complex.

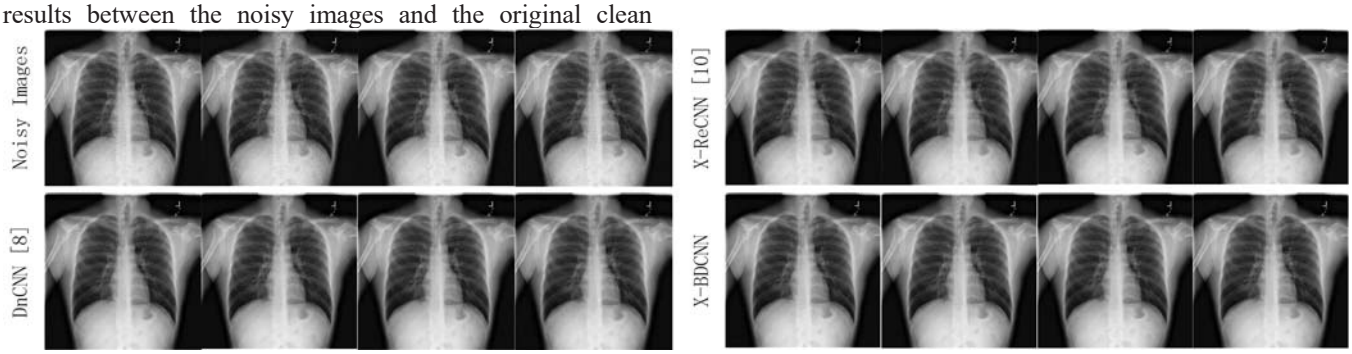

Fig. 2. Result of different denoising methods on the synthetic X-ray images with strong noise of different (η, σ). The top-left row is the noise image with (η, σ) equal to (0.4, 10), (0.4, 15), (0.6, 10), (0.6, 15) respectively. The other images from top-right to bottom-right is the corresponding denoised images by different methods, respectively. For more details please enlarge the figure.

TABLE I THE QUANTITATIVE RESULTS ON THE TEST SET BY VARIOUS DENOISING METHODS UNDER DIFFERENT NOISE LEVELS. BEST RESULTS ARE HIGHLIGHT IN BOLD.

Methods	SNR	PSNR	SSIM	Time (s)
Before Denoising	18.8836	24.1916	0.51	-
BM3D [5]	29.2848	34.5929	0.8639	0.152
DnCNN [8]	40.3754	35.372	0.9822	0.005
X-ReCNN [10]	38.4869	33.59	0.974	**0.004**
X-BDCNN	**41.1070**	**36.1196**	**0.9838**	0.006
X-BDCNN w/o SSIM loss	40.9966	35.8403	0.9838	0.006
X-BDCNN w/o the NLE	40.9609	35.945	0.9837	0.005

In order to verify the performance of the NLE subnetwork and the SSIM loss function, we further train X-BDCNN without the NLE subnetwork and without SSIM loss to conduct ablation experiments, respectively. The experimental results can be seen in Table I. Comparing with X-BDCNN, it does not achieve the best performance when the NLE subnetwork or SSIM loss is removed from X-BDCNN. Meanwhile, it's easy to find that both X-BDCNN without the NLE subnetwork and X-BDCNN without SSIM loss have a better performance than the other methods. This indicates that both the NLE subnetwork and SSIM loss can boost the performance of X-BDCNN. The biggest difference between X-BDCNN without the NLE subnetwork and the other CNN-based methods is that whether there is a noise level estimation subnetwork besides the architecture and loss function. However, the results of X-BDCNN without the NLE subnetwork is better than the others. Therefore, a noise level estimation subnetwork is necessary for denoising.

To further investigate the stability of X-BDCNN, we randomly select 10 chest X-ray images (1024×1024) from the ChestX-ray8 [14] to conduct the experiments under the strong hybrid noise with $\eta \in (0.4, 0.6, 0.8)$ and $\sigma \in (5, 10, 15)$.

TABLE II THE AVERAGE SNR/PSNR/SSIM RESULTS BY DIFFERENT METHODS UNDER DIFFERENT NOISE LEVELS. BEST RESULTS ARE HIGHLIGHT IN BOLD.

Noise Level (η, σ) (PSNR)	DnCNN [8]	X-ReCNN [10]	X-BDCNN
(0.4, 5) (22.5162)	39.5037/35.2209/0.9832	36.9640/32.6811/0.9758	**40.1925/35.9096/0.9848**
(0.6, 5) (24.0733)	40.1841/35.9012/0.9848	37.6373/33.3545/0.9786	**40.8287/36.5459/0.9861**
(0.8, 5) (25.1555)	40.6018/36.3189/0.9858	37.9762/33.6934/0.9799	**41.2326/36.9498/0.9868**
(0.4, 10) (21.7703)	39.1050/34.8221/0.9821	36.5160/32.2331/0.9724	**39.8214/35.5385/0.9840**
(0.6, 10) (23.0213)	39.6908/35.4080/0.9835	37.1694/32.8865/0.9754	**40.3547/36.0718/0.9850**
(0.8, 10) (23.8439)	40.0154/35.7326/0.9842	37.4960/33.2131/0.9768	**40.6748/36.3919/0.9856**
(0.4, 15) (20.7651)	38.5502/34.2673/0.9805	35.6645/31.3816/0.9594	**39.3198/35.0369/0.9828**
(0.6, 15) (21.7165)	39.0246/34.7418/0.9816	36.3036/32.0207/0.9634	**39.7464/35.4635/0.9836**
(0.8, 15) (22.2952)	39.2669/34.9841/0.9822	36.6005/32.3176/0.9652	**39.9653/35.6824/0.9840**

The results are shown in TABLE II. It can be found that our method and the contrasted methods can restore the noisy image corrupted by strong hybrid Poisson-Gaussian noise. Additionally, X-BDCNN has best performance on dealing with noisy image with different noise levels in the evaluation criteria of the average SNR, PSNR and SSIM. The Fig. 2 shows the denoising results of the three methods on one X-ray image corrupted by different noise intensity. We find that the X-ray image denoised by X-ReCNN [10] has some noise spot. Comparing with the X-ReCNN [10] and the DnCNN [8], the denoised image by X-BDCNN has a better visual results with more structural information.

IV. Conclusion

Aiming at the problem that low-dose X-ray images have little harm to the human body but often are with noise, we have proposed an image denoising method X-BDCNN for low-dose X-ray images. To guarantee the application of X-BDCNN for realistic noisy X-ray images, we build a hybrid Poisson-Gaussian noise model for low-dose X-ray images by combining the physical principles of X-ray imaging under a low radiation dosage. Our X-BDCNN is comprised of the NLE subnetwork and the NBD subnetwork, where the estimated noise level by the NLE subnetwork is used to assist the NBD subnetwork to improve the denoising performance. To guarantee the structural information of denoised X-ray images, the SSIM is integrated into the loss function for training X-BDCNN. Extensive experiments on synthetic images have demonstrated the good performance of X-BDCNN in terms of quantitative quality evaluations. Though we only test the performance of X-BDCNN on X-ray images, X-BDCNN is probably applicable to other medical images similar to X-ray imaging, such as computed tomography scans. It is worth remarking that our proposed hybrid Poisson-Gaussian noise model may be different from the actual noise model of low-dose X-ray images. Therefore, the more accurate noise model of low-dose X-ray images should be studied to generate training data for training deep learning-based denoising methods.

Acknowledgment

This work was supported in part by Zhejiang Provincial Natural Science Foundation of China (LQ20F030013), Research Foundation of HwaMei Hospital, University of Chinese Academy of Sciences, China (2020HMZD22), Ningbo Public Service Technology Foundation, China (202002N3181), and Medical Scientific Research Foundation of Zhejiang Province, China (2021431314).

References

[1] R. Smith-Bindman, J. Lipson, R. Marcus, K.-P. Kim, M. Mahesh,R. Gould, A. B. De Gonz´alez, and D. L. Miglioretti, "Radiation doseassociated with common computed tomography examinations and theassociated lifetime attributable risk of cancer,"Archives of internalmedicine, vol. 169, no. 22, pp. 2078–2086, 2009

[2] T. B. Chandra and K. Verma, "Analysis of quantum noise-reducing filters on chest x-ray images: A review," Measurement, vol. 153, p. 107426, 2020.

[3] L. I. Rudin, S. Osher, and E. Fatemi, "Nonlinear total variation based noise removal algorithms," Physica D: nonlinear phenomena, vol. 60, no. 1-4, pp. 259–268, 1992.

[4] A. Buades, B. Coll, and J.-M. Morel, "A non-local algorithm for image denoising," in 2005 IEEE Computer Society Conference on Computer Vision and Pattern Recognition (CVPR'05), vol. 2. IEEE, 2005, pp. 60–65.

[5] K. Dabov, A. Foi, V. Katkovnik, and K. Egiazarian, "Image denoising by sparse 3-d transform-domain collaborative filtering," IEEE Transactions on image processing, vol. 16, no. 8, pp. 2080–2095, 2007.

[6] J. Salmon, Z. Harmany, C.-A. Deledalle, and R. Willett, "Poisson noise reduction with non-local pca," Journal of mathematical imaging and vision, vol. 48, no. 2, pp. 279–294, 2014.

[7] L. Azzari and A. Foi, "Variance stabilization for noisy+ estimate combination in iterative poisson denoising," IEEE signal processing letters, vol. 23, no. 8, pp. 1086–1090, 2016.

[8] K. Zhang, W. Zuo, Y. Chen, D. Meng, and L. Zhang, "Beyond a gaussian denoiser: Residual learning of deep cnn for image denoising," IEEE Transactions on Image Processing, vol. 26, no. 7, pp. 3142–3155, 2017.

[9] S. Guo, Z. Yan, K. Zhang, W. Zuo, and L. Zhang, "Toward convolutional blind denoising of real photographs," in Proceedings of the IEEE Conference on Computer Vision and Pattern Recognition, 2019, pp. 1712–1722.

[10] Y. Jin, X.-B. Jiang, Z.-k. Wei, and Y. Li, "Chest x-ray image denoising method based on deep convolution neural network," IET Image Processing, vol. 13, no. 11, pp. 1970–1978, 2019.

[11] S. Dutta, S. Chaturvedi, S. Kumar, and M. Bhatia, "Skidnet: Skip image denoising network for x-rays," in 2019 International Joint Conference on Neural Networks (IJCNN). IEEE, 2019, pp. 1–8.

[12] O. Ronneberger, P. Fischer, and T. Brox, "U-net: Convolutional networks for biomedical image segmentation," in International Conference on Medical image computing and computer-assisted intervention. Springer, 2015, pp. 234–241.

[13] Y. Lu, R. W. Liu, F. Chen, and L. Xie, "Learning a deep convolutional network for speckle noise reduction in underwater sonar images," in Proceedings of the 2019 11th International Conference on Machine Learning and Computing, 2019, pp. 445–450.

[14] X. Wang, Y. Peng, L. Lu, Z. Lu, M. Bagheri, and R. M. Summers, "Chestx-ray8: Hospital-scale chest x-ray database and benchmarks on weakly-supervised classification and localization of common thorax diseases," in Proceedings of the IEEE Conference on Computer Vision and Pattern Recognition (CVPR), July 2017.